Probing QFS mechanism with the 12C(p, 2p)11B reaction in inverse kinematics

Phys. Lett. B 879 (2026) 140595

Contents lists available at ScienceDirect

Physics Letters B

journal homepage: www.elsevier.com/locate/physletb

Letter

Probing QFS mechanism with the $^{12}C(p,2p)^{11}B$ reaction in inverse kinematics

V. Panin [a,b,*], M. Holl [b], J. T. Taylor [c], Y. Aksyutina [a], H. Alvarez-Pol [d], T. Aumann [b,a,e], C. A. Bertulani [f,e], K. Boretzky [a], C. Caesar [b], M. Chartier [c], L. V. Chulkov [g], D. Cortina-Gil [d], J. Enders [b,e], O. Ershova [h], H. Geissel [a,1], R. Gernhäuser [i], M. Heil [a], H. T. Johansson [j], B. Jonson [j], A. Kelić-Heil [a], C. Langer [h], T. Le Bleis [i], R. Lemmon [k,1], T. Nilsson [j], O. Kiselev [a], S. Paschalis [l,b], M. Petri [l,b], R. Plag [a], R. Reifarth [h], D. Rossi [b,a], H. Scheit [b], H. Simon [a], F. Wamers [b,a], H. Weick [a], C. Wimmer [h]

[a] GSI Helmholtzzentrum für Schwerionenforschung, Darmstadt, 64291, Germany
[b] Institut für Kernphysik, Technische Universität Darmstadt, Darmstadt, 64289, Germany
[c] Oliver Lodge Laboratory, University of Liverpool, Liverpool, L69 7ZE, United Kingdom
[d] IGFAE, Instituto Galego de Física de Altas Enerxías, Universidade de Santiago de Compostela, Santiago de Compostela, E-15782, Spain
[e] Helmholtz Forschungsakademie Hessen für FAIR (HFHF), GSI Helmholtzzentrum für Schwerionenforschung, Darmstadt, 64291, Germany
[f] Department of Physics and Astronomy, East Texas A&M University, Commerce, Texas, 75429, USA
[g] NRC Kurchatov Institute, Moscow, Ru-123182, Russia
[h] Goethe-Universität Frankfurt am Main, Frankfurt am Main, 60438, Germany
[i] Physik Department E12, Technische Universität München, Garching, 85748, Germany
[j] Institutionen för Fysik, Chalmers Tekniska Högskola, Göteborg, S-412 96, Sweden
[k] STFC Daresbury Laboratory, Daresbury, Warrington, WA4 4AD, United Kingdom
[l] School of Physics, Engineering and Technology, University of York, York, YO10 5DD, United Kingdom

ARTICLE INFO

Editor: Silvia Monica Lenzi

Keywords:
Quasi-free scattering
Nucleon knockout
Treiman-Yang test

ABSTRACT

The reaction mechanism of the quasi-free scattering (QFS) reaction $^{12}C(p,2p)^{11}B$ is investigated in inverse and complete kinematics using a ^{12}C beam at 400 MeV/nucleon impinging on a polyethylene (CH_2) target. A complete set of kinematic observables characterizing the three-body final state is obtained through the exclusive reconstruction of the ^{11}B recoil fragment and the two outgoing protons. For the first time, a systematic Treiman-Yang test is applied to inverse-kinematics $(p,2p)$ reactions with a heavy-ion beam, taking advantage of the large phase space covered by the experimental setup, particularly in non-coplanar kinematic configuration. This model-independent test confirms the predominance of the QFS reaction mechanism. The characteristic dependence of the Treiman-Yang angle on the azimuthal correlation of the outgoing protons, along with other kinematic signatures, provides further evidence for the single-step proton knockout process.

1. Introduction

Quasi-free scattering (QFS) reactions induced by relativistic radioactive-ion beams on hydrogen targets have emerged as a powerful tool in modern nuclear physics, enabling the extraction of structural information on exotic and stable nuclei from experimental observables [1,2]. In recent years, QFS reactions have provided numerous experimental insights into diverse nuclear phenomena, including shell evolution in isospin-asymmetric nuclei [3–6], the structure of weakly-bound few-body systems [7], short-range nucleon-nucleon correlations [8,9], alpha clustering [10] and such exotic systems as the elusive tetraneutron [11] and nuclei beyond the neutron drip line [12].

In particular $(p,2p)$ and (p,pn) cross sections are instrumental for quantifying the occupation probabilities of single-particle proton and neutron orbitals [1,13,14]. They provide an important input to understanding the shell structure and nucleon correlations in both stable and exotic systems. At the same time the interpretation of the cross sections is inherently model-dependent, as it relies on the accuracy of the

* Corresponding author.
E-mail address: V.Panin@gsi.de (V. Panin).
[1] Deceased

https://doi.org/10.1016/j.physletb.2026.140595
Received 27 December 2025; Received in revised form 24 May 2026; Accepted 25 May 2026
Available online 26 May 2026

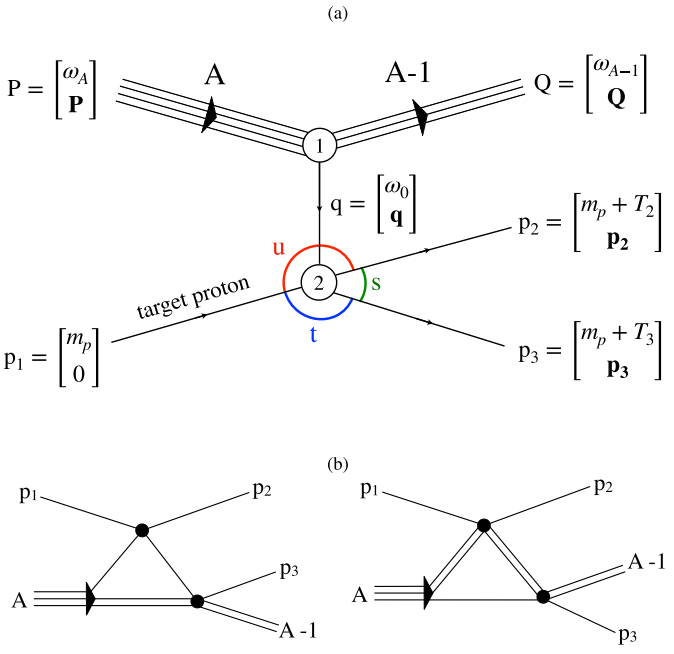

Fig. 1. (a): One-step QFS mechanism of a $(p,2p)$ reaction. The process is described as elastic p-p scattering of a virtual proton with 4-momentum q, bound inside the nucleus A, off the target proton p_1. The definitions of the energies and momenta are given in the laboratory frame (see text for more details). (b): Triangular diagrams for possible secondary processes which lead to the same three particles in the final state. A process with two protons interacting in the final state is not shown although it can also contribute to FSI.

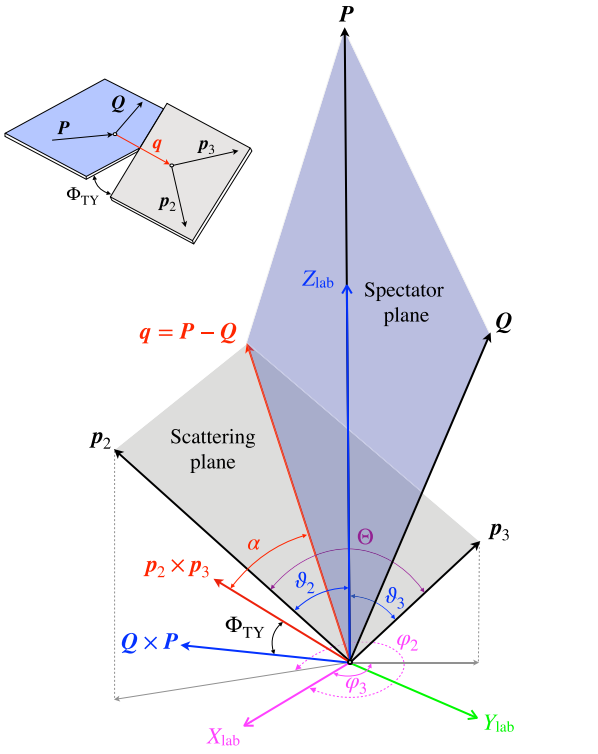

Fig. 2. The definition of a coordinate system for $(p,2p)$ reactions in inverse kinematics. The laboratory Z axis coincides with the momentum $\boldsymbol{P}$ of the projectile nucleus A. $\vartheta_{2,3}$ and $\varphi_{2,3}$ are the laboratory polar and azimuth angles of the outgoing protons with momenta $\boldsymbol{p}_2$ and $\boldsymbol{p}_3$. The spectator plane in which $\boldsymbol{P}$ and the momentum of the (A-1) fragment $\boldsymbol{Q}$ as well as the momentum of the virtual proton $\boldsymbol{q}$ are coplanar is shown by blue shaded area. The gray-shaded area is a scattering plane in which vectors $\boldsymbol{q}$, $\boldsymbol{p}_2$ and $\boldsymbol{p}_3$ are also coplanar. The vector $\boldsymbol{q}$ lies at the intersection of the two kinematic planes. The inset figure shows the spectator and scattering planes rotated by the Treiman-Yang angle $\Phi_{\rm TY}$ about the momentum of the virtual proton $\boldsymbol{q}$.

underlying reaction theory - specifically, its ability to account for distortion effects due to initial- and final-state interactions (ISI/FSI) and the applicability of the impulse approximation [15–17].

From experimental standpoint, isolating genuine QFS events (as depicted in Fig. 1a) is another significant challenge. These true one-step reactions must be disentangled from contributions arising from ISI/FSI (Fig. 1b) or simply from experimental background. To ensure meaningful comparison with theoretical models, it is therefore crucial to apply stringent event selection and validation criteria grounded on the impulse approximation and relativistic kinematics [18,19] .

Here we discuss selected kinematic tests of the QFS reaction mechanism for the benchmark reaction ^{12}C$(p,2p)^{11}$B in inverse kinematics, when all three final-state products (the two protons and the ^{11}B fragment) are measured simultaneously. While extending this methodology to other types of QFS reactions such as (p,pn), (p,pd), $(p,p\alpha)$ is conceptually straightforward, it remains poorly investigated experimentally. The systematic approach presented here may help to pave the way for similar studies in other QFS experiments.

2. Experimental considerations

The customary approach in inverse-kinematics $(p,2p)$ experiments involves measurements of outgoing protons with large acceptance and high efficiency using a calorimetric method, *i.e.* when protons deposit energy in thick detectors behind a hydrogen target [20–22]. The significant probability for high-energy protons to punch through even very thick materials, depositing only a fraction of the full kinetic energy, may limit the energy range and accuracy of such experiments. Besides that the measurements often lack the missing-energy resolution found in direct-kinematics experiments, where protons are measured with high resolution but rather limited acceptance, using magnetic spectrometers [14]. Additional challenges stem from the acceptance constraints imposed by an experimental apparatus and a choice of appropriate variables for evaluating phase-space integrals and the acceptance corrections [10,23].

Inverse-kinematics offers a possibility to obtain spectroscopic data from redundant observation of (A-1) spectator system or its decay products, while the detection of the outgoing pair of protons serves primarily as a reaction trigger (see, *e.g.*, [24]). In this case, the QFS mechanism manifests as a narrow correlation of the polar angles ϑ_2 and ϑ_3 of the outgoing protons (p_2 and p_3 in Fig. 1a) at a nearly constant relative (opening) angle Θ defined as:

$$\cos\Theta = \frac{\boldsymbol{p}_2\cdot\boldsymbol{p}_3}{|\boldsymbol{p}_2||\boldsymbol{p}_3|} = \sin\vartheta_2\sin\vartheta_3\cos(\varphi_2-\varphi_3)+\cos\vartheta_2\cos\vartheta_3, \quad (1)$$

where $\boldsymbol{p}_2$ and $\boldsymbol{p}_3$ are the laboratory 3-momenta of the protons, φ_2 and φ_3 are their azimuth angles (see Fig. 2). Another QFS signature related to the underlying two-body process can be found in the azimuthal difference $\Delta\varphi = \varphi_2$-$\varphi_3$ centered at π.

Strictly speaking, Θ and $\Delta\varphi$ alone do not provide an unambiguous identification of the one-step QFS mechanism illustrated by the diagram in Fig. 1a. The experimental distributions of Θ and $\Delta\varphi$ usually span across several degrees due to Fermi momentum, binding energy, experimental resolutions and individual kinematic scenarios. This leads to uncertainties with respect to ISI/FSI which may contaminate the same observation range (see, *e.g.*, [25]). Furthermore, above certain energies the inelastic p-p interactions need to be taken into account as well Patsyuk et al. [9].

Inverse kinematics provides a suitable configuration to test the QFS mechanism using a limited set of kinematic observables *e.g.* without accurate energy measurements of the protons in the final state. Here, we

apply this approach to the reaction $^{12}C(p,2p)^{11}B$ measured with a ^{12}C beam at 400 MeV/nucleon impinging on a CH_2 target as reported in our earlier publication [21]. The outgoing protons were measured within a large solid angle in the laboratory frame, covering $\varphi_{2,3} \in [0, 2\pi]$ in the azimuthal direction and $\vartheta_{2,3} \in [20°, 60°]$ in the polar direction. Combined with the exclusive detection of the outgoing ^{11}B fragment, this enables a validity test of the QFS pole factorization, using the well established Treiman-Yang (TY) test [26].

3. Inverse-kinematics observables

The definition of the kinematical quantities in QFS reactions can be found *e.g.* in refs. [23,27,28]. In the usual impulse approximation, $(p, 2p)$ reactions can be described by the diagram in Fig. 1a. A virtual proton with 3-momentum $\boldsymbol{q}$ is bound inside a projectile nucleus with mass M_A which has the laboratory momentum $\boldsymbol{P} = (0, 0, P_z)$. The spectator fragment with mass M_{A-1} has laboratory 3-momentum $\boldsymbol{Q} = (Q_x, Q_y, Q_z)$. Hence, the total energy of the virtual (bound) proton can be defined in the lab frame as

$$\omega_0 = \omega_A - \omega_{A-1} = \sqrt{M_A^2 + P^2} - \sqrt{(M_{A-1} + E_x)^2 + Q^2}, \tag{2}$$

where E_x is the excitation energy of the (A-1) spectator, corresponding to the proton-hole state.

In the scattering pole (vertex 2 in Fig. 1a), the virtual proton interacts with the target proton at rest ($\boldsymbol{p}_1 = 0$). Two free protons with the laboratory momenta $\boldsymbol{p}_2$ and $\boldsymbol{p}_3$ are emitted in the final state. Momentum conservation leads to the following relation for the 3-momentum $\boldsymbol{q}$ of the virtual proton in the lab frame

$$\boldsymbol{q} = \boldsymbol{P} - \boldsymbol{Q} = \boldsymbol{p}_2 + \boldsymbol{p}_3. \tag{3}$$

Combining this with Eq. (2), the off-shell mass μ of the virtual proton can be writen as

$$\mu = \sqrt{\omega_0^2 - \boldsymbol{q}^2}, \tag{4}$$

and from the energy conservation in the p-p process it follows that

$$\omega_0 = m_p + T_2 + T_3, \tag{5}$$

where $T_{2,3}$ are the kinetic energies of outgoing protons in the lab frame, and m_p is the proton mass.

An important consequence of Eq. (3) is that $\boldsymbol{q}$ is simultaneously coplanar with every pair of vectors ($\boldsymbol{p}_2$, $\boldsymbol{p}_3$) and ($\boldsymbol{P}$, $\boldsymbol{Q}$). This can be written as a scalar product

$$\cos\alpha = \frac{(\boldsymbol{p}_2 \times \boldsymbol{p}_3)}{|\boldsymbol{p}_2 \times \boldsymbol{p}_3|} \cdot \frac{\boldsymbol{q}}{|\boldsymbol{q}|} = 0, \tag{6}$$

where α is the angle between the normal vector of the p-p scattering plane and $\boldsymbol{q}$. In the case of an ideal QFS mechanism the distribution of α should be a δ-function at $\pi/2$. Due to the experimental resolutions one may expect instead a narrow distribution around $\pi/2$ that provides an additional QFS signature.

Fig. 3(a) shows the experimental distributions of α for the reaction $^{12}C(p,2p)^{11}B$. A narrow peak around 90° corresponds to hydrogen-induced reactions in the CH_2 target. The rms peak width from a Gaussian fit is $\sigma \approx 1.4°$ due to the experimental resolution. The reactions induced by the carbon component of the CH_2 were measured with a pure carbon target, which resulted in a much broader distribution as shown in the same figure. Gating on the $\alpha = 90°$ peak, the carbon-induced background can be largely suppressed. In the following discussion the gate $85° < \alpha < 95°$ is applied everywhere. This corresponds to a background-to-signal ratio of around 1/11 compared to 1/6 when no such condition is used.

The coplanarity of the three vectors $\boldsymbol{q}$, $\boldsymbol{p}_2$ and $\boldsymbol{p}_3$ can also be examined by transforming to a rotated reference frame - hereafter referred as a "q-frame" - which is defined on an event-by-event basis such that its polar Z-axis is aligned with the direction of $\boldsymbol{q}$. In Fig. 3 the angular distributions of the two protons in the q-frame (red empty circles) are compared to the analogous distributions in the laboratory frame (blue filled circles). In Fig. 3b the relative (opening) angle Θ is compared to a simple sum of polar angles calculated either in the laboratory frame as $\vartheta_2^{\rm lab} + \vartheta_3^{\rm lab}$ or in the q-frame as $\vartheta_2^q + \vartheta_3^q$, where it effectively coincides with Θ. Similarly, Fig. 3c and d compare the azimuthal distributions in the q-frame and laboratory frame. Narrow azimuthal distributions in the q-frame reflect the appropriate frame's rotation which compensates the broadening effect caused by the nuclear Fermi motion.

Besides the coplanarity condition, which may partly reflect a trivial kinematic correlation among the three particles in the final state, it is also essential to examine the relative rotation of the spectator and scattering planes about the vector $\boldsymbol{q}$. This constitutes the core of the Treiman-Yang test discussed in Section 4. As discussed in refs. [23,29], the impulse approximation can break down under certain conditions due to the complex spin and angular-momentum structure of the reaction amplitude, as well as possible final-state interactions, that should be reflected in the distribution of the Treiman-Yang angle. For the detailed analysis, we rely on the reconstruction of the complete reaction kinematics as presented below.

The QFS kinematics can be conveniently formulated in the invariant form using the formalism of Mandelstam variables. Following the approach similar to Stetz [23], Debebe et al. [28] and applying notations for the four-momenta $p_{1,2,3}$ and q as in Fig. 1a, the full system of equations for the p-p scattering pole can be written as

$$s = (p_2 + p_3)^2 = (q + p_1)^2 = \mu^2 + m_p^2 + 2\omega_0 m_p, \tag{7}$$

$$t = (q - p_2)^2 = (p_1 - p_3)^2 = -2m_p T_3, \tag{8}$$

$$u = (q - p_3)^2 = (p_1 - p_2)^2 = -2m_p T_2, \tag{9}$$

$$s + t + u = 3m_p^2 + \mu^2, \tag{10}$$

where $T_{2,3}$ are the laboratory kinetic energies of the outgoing protons. The proportionality between the invariants t and u and $T_{2,3}$ is a characteristic feature of the inverse kinematics. At the same time t and u define the scattering angles of the two protons.

In the present experiment, an accurate measurement of $T_{2,3}$ was not feasible due to high probability of protons to punch through the calorimeter and the lack of a reliable energy calibration method for these events. Instead, $T_{2,3}$ were reconstructed by combining the recoil momentum $\boldsymbol{Q}$ with the angular information of the outgoing protons. This can be done, *e.g.*, by expanding and solving Eqs. (8) and (9)

$$T_{2(3)} = \frac{A E_{\rm tot} \pm q\cos\theta_{q2(3)} \sqrt{A^2 - m_p^2 (E_{\rm tot}^2 - q^2 \cos^2\theta_{q2(3)})}}{E_{\rm tot}^2 - q^2\cos^2\theta_{q2(3)}} - m_p, \tag{11}$$

where

$$A = \omega_0 m_p + \frac{\mu^2 + m_p^2}{2}, \text{ and} \tag{12}$$

$$E_{\rm tot} = \omega_0 + m_p, \tag{13}$$

and the relative angles of the pairs of laboratory vectors ($\boldsymbol{q}$,$\boldsymbol{p}_2$) and ($\boldsymbol{q}$,$\boldsymbol{p}_3$) are defined as θ_{q2} and θ_{q3}, respectively. Only the positive sign in front of the square root is adopted following the prescription from Baldin et al. [30]. Eq. (11) can be generalized for a QFS knockout of any other nuclear constituent by substituting appropriate masses.

Using $T_{2(3)}$, the scattering angle θ_{pp}^* in the p-p center-of-mass frame can be calculated from

$$\cos\theta_{pp}^* = \sqrt{\frac{s}{s - 4m^2}} \frac{2m(T_3 - T_2)}{\lambda^{1/2}(s, \mu^2, m^2)}, \tag{14}$$

where $\lambda(s, \mu^2, m^2)$ is a Källén triangle function [31]

$$\lambda(x, y, z) \equiv (x - y - z)^2 - 4yz. \tag{15}$$

The off-shell mass μ and the Mandelstam variable s are determined by the (A-1) fragment (Eqs. (4) and (7)) and thus can be obtained from the experimental data. Due to the random choice of indices for the two (indistinguishable) protons in Eq. (14) the distribution of θ_{pp}^* is symmetric with respect to $\pi/2$.

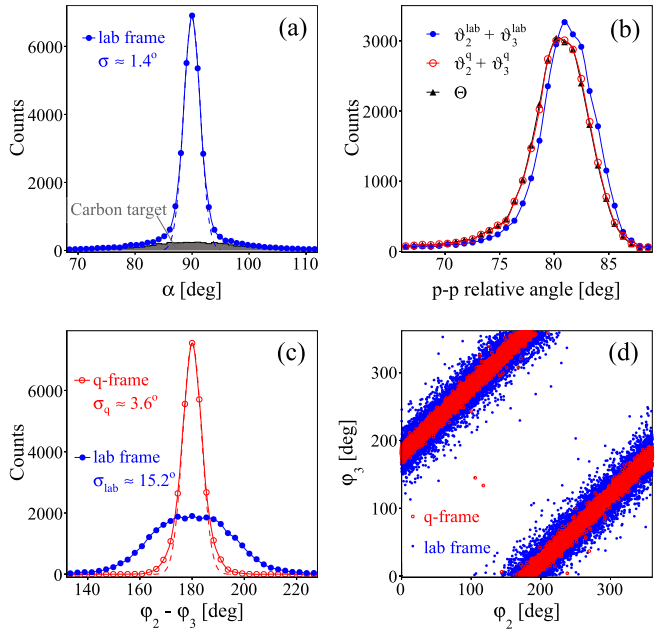

Fig. 3. Angular distributions of the final state products from $^{12}C(p, 2p)^{11}B$ reaction in inverse kinematics. (a): distribution of the angle α (Eq. (6)) measured with CH_2 (blue filled circles) and carbon target (grey shaded area) where $\sigma \approx 1.4°$ is the width of the Gauss fit to the CH_2 data (dashed blue line). Figures b,c and d compare angular distributions in the q-frame (red empty circles) with the analogous distributions in the laboratory frame (blue filled circles). The gate $85° < \alpha < 95°$ is applied in figures b,c and d. In (c) the inset values of σ_q and σ_{lab} correspond to the widths of the Gauss fit to the distributions in the q-frame and lab frame, respectively.

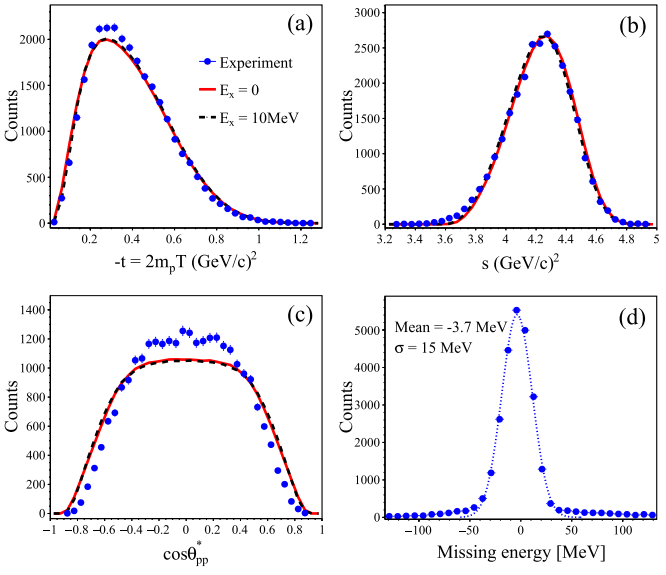

Fig. 4. Experimental distributions (blue points) of the Mandelstam variables t and s, the center-of-mass p-p scattering angle θ^*_{pp} and the missing energy calculated from Eq. (16). Solid red and dashed black curves are the simulations corresponding to the population of the ^{11}B ground state and a 10 MeV state, respectively. The missing-energy spectrum shows the Gaussian fit (dashed line) with the corresponding fit values. The simulations incorporate all experimental resolutions, acceptances, etc., and are plotted with the same binning and scaled to the same integrals as the experimental data.

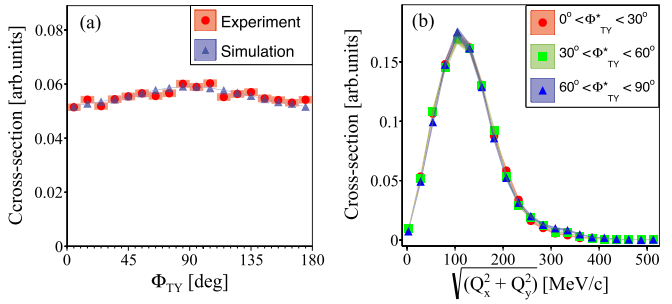

Fig. 5. Left: Distribution of Φ_{TY} from the $^{12}C(p, 2p)^{11}B$ reaction in comparison to the simulation (both normalized to unity). Right: experimental distributions of the transverse momentum of the ^{11}B fragment within different ranges of Φ^*_{TY}, where each distribution is normalized to integrated counts from the corresponding Φ^*_{TY} range.

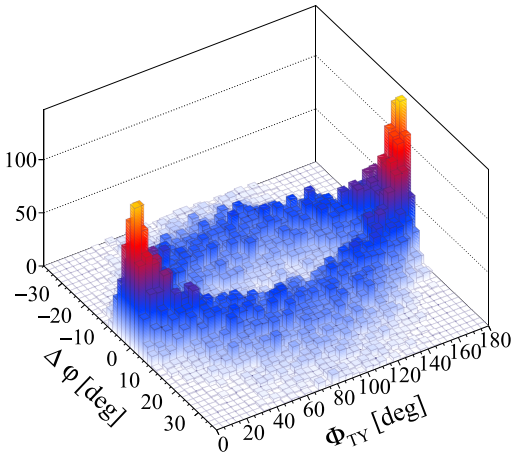

Fig. 6. Experimental correlation between Φ_{TY} and the azimuthal difference of the two protons $\Delta\varphi = \varphi_2 - \varphi_3 - 180°$ in the laboratory reference frame for the $^{12}C(p, 2p)^{11}B$ reaction in inverse kinematics.

Fig. 4 shows reconstructed t, s and θ^*_{pp} distributions in comparison with Monte-Carlo simulations based on the relativistic QFS kinematics code developed in Panin et al. [21], Chulkov et al. [27]. The simulations take into account all experimental cuts, detector resolutions and geometrical acceptances determined with the help of Geant4. The procedure to analyze simulated events is the same as for the experimental data. The resulting rms resolutions for θ^*_{pp} and t are estimted to be around 3.3° and 0.05 (GeV/c)^2, respectively. The p-p cross section in the simulation is taken to be constant and isotropic in the p-p center-of-mass frame, while a certain degree of anisotropy may need to be incorporated to achieve a more accurate reproduction of $\cos\theta^*_{pp}$ distribution in Fig. 4c.

The reconstructed reaction kinematics is based on the assumption that ^{11}B is populated in the ground state, *i.e.*, that the excitation energy $E_x = 0$ is used in the calculation of ω_0 (Eq. (2)). To assess the effect of this approximation, Fig. 4 shows additional kinematic curves for the reaction with $E_x = 10$ MeV, reconstructed under the assumption $E_x = 0$. The resulting deviations are found to be well within the limits of the experimental resolution.

For the final consistency check, the missing energy E_{miss} is calculated from

$$E_{miss} = \sqrt{(p_1 + P - p_2 - p_3)^2} - M_{11_B}, \quad (16)$$

where $p_{1,2,3}$ and P are 4-vectors depicted in Fig. 1a. The corresponding 3-vectors $\boldsymbol{p_2}$ and $\boldsymbol{p_3}$ are reconstructed using measured proton angles and calculated kinetic energies from Eq. (11). Fig. 4d shows the resulting missing-energy distribution with Gaussian rms width $\sigma \approx 15$ MeV, which reflects the experimental resolution.

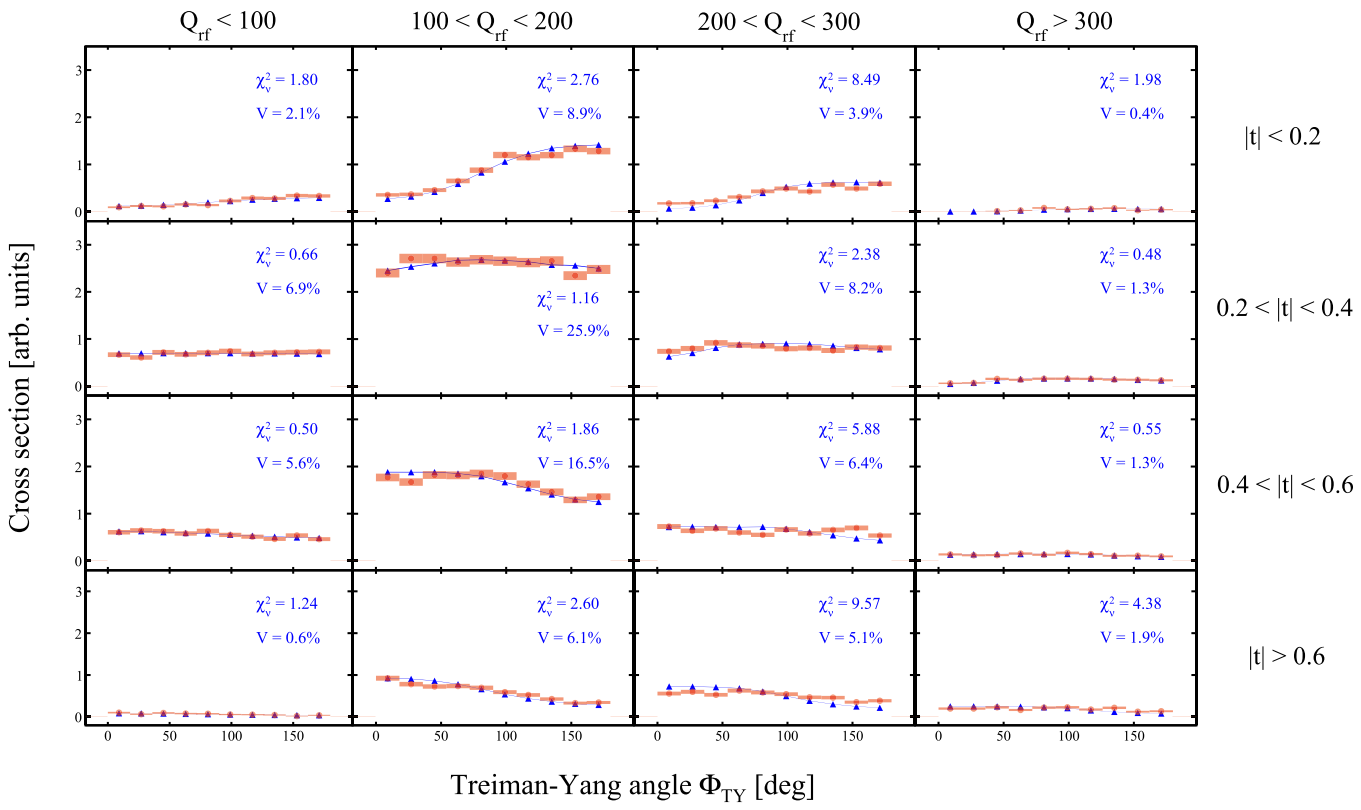

Fig. 7. Distribution of the Treiman-Yang angle Φ_{TY} for different ranges of the momentum transfer t and different magnitudes of the ^{11}B recoil momentum Q_{rf} in the rest frame of ^{12}C projectile. The selected ranges for Q_{rf} (in MeV/c units) and t (in (GeV/c)^2 units) are indicated for the corresponding columns and rows on top and on the right side of the figure, respectively. The experimental data is shown by red circles with the vertical error bars representing the statistical uncertainties. Blue triangles correspond to the simulations which take into account the experimental acceptance and resolutions of all final-state products. The simulation is based on the idealized QFS reaction mechanism described by the diagram in Fig. 1a. The statistical errors of the simulations are within the point symbols.

Although such kinematic reconstruction is not suitable for precise missing-energy spectroscopy of populated proton-hole states, it provides a practical means to explore the phase space of the three-body final state. In particular, it enables a systematic test of the impulse approximation across different kinematic regions by examining the corresponding distributions of the Treiman-Yang angle.

4. The Treiman-Yang test

The Treiman-Yang (TY) test offers an experimental probe of the pole factorization illustrated by the diagram in Fig. 1a. Originally suggested for single-pion exchange reactions [26], the TY test was later generalized [32] for other processes where an exchange particle can have spin 1/2, assuming that non-polarized targets and projectiles are used. The TY test has been applied to study the mechanism of various types of nuclear reactions [33–36] and, in particular, has been proposed as a useful approach in QFS knockout experiments [23]. The test aims at obtaining a distribution of the angle Φ_{TY} which can be defined in Fig. 2 as the rotation angle between the two reaction planes around the momentum of the virtual particle $\boldsymbol{q}$. The angle Φ_{TY} can be calculated using

$$\cos\Phi_{TY} = \frac{\boldsymbol{P}\times\boldsymbol{Q}}{|\boldsymbol{P}\times\boldsymbol{Q}|}\cdot\frac{\boldsymbol{p_2}\times\boldsymbol{p_3}}{|\boldsymbol{p_2}\times\boldsymbol{p_3}|}. \quad (17)$$

If the QFS factorization holds, no correlation is expected between the (A-1) spectator and the scattered protons beyond what follows from the kinematics, and thus the reaction cross sections should be independent on Φ_{TY}. At the same time, any significant contribution of ISI/FSI, such as those illustrated by the triangular diagrams in Fig. 1b or any other breakdown of the impulse approximation, should lead to observable distortions [29].

The experimental ^{12}C$(p,2p)^{11}$B cross sections in Fig. 5a are found to be rather uniform over the full range of Φ_{TY} which asserts the underlying QFS factorization. A moderate enhancement (around 10%) in the vicinity of $\Phi_{TY} = 90°$ is well reproduced by the simulations taking into account the experimental acceptances and resolutions. Due to the random choice of the indices 2 and 3 for the final-state protons, the Φ_{TY} distribution is symmetric with respect to $\pi/2$ and thus can be replaced by a reduced angle $\Phi^*_{TY} \in [0, \pi/2]$ defined as

$$\Phi^*_{TY} = \pi/2 - |\Phi_{TY} - \pi/2|. \quad (18)$$

Fig. 5b shows that experimental momentum distributions of ^{11}B fragment are remarkably independent on Φ^*_{TY}. This can be seen as another manifestation of the TY criterion despite the fact that large momentum components prevail in the non-coplanar region [21], where Φ^*_{TY} is close to 90°. Fig. 6 illustrates the experimental dependency of Φ_{TY} on the azimuthal difference $\Delta\varphi = \varphi_2 - \varphi_3 - 180°$, where non-coplanar kinematics clearly dominates around $\Phi_{TY} = 90°$.

Owing to the large phase space covered by the experimental setup, it is possible to inspect TY distributions for various kinematic cases. Of particular interest are the regions near extremes of the momentum transfer t and at large rest-frame momentum $\boldsymbol{Q}_{rf}$, where substantial deviations from the simple pole approximation can be expected, as discussed in Kolybasov et al. [29]. $\boldsymbol{Q}_{rf}$ is obtained by the Lorentz boost of the ^{11}B laboratory momentum $\boldsymbol{Q} = (Q_x, Q_y, Q_z)$ into the rest frame of the ^{12}C projectile:

$$\boldsymbol{Q}_{rf} = (Q_x,\ Q_y,\ \gamma(Q_z - \beta(M^2_{^{11}\mathrm{B}} + Q^2)^{1/2}), \quad (19)$$

where $M_{^{11}\mathrm{B}}$ is the mass of ^{11}B, β and γ correspond to the velocity and the Lorentz factor of the incident ^{12}C beam, respectively.

Fig. 7 shows Φ_{TY} distributions for simultaneously varied ranges of t and Q_{rf}, and compares them to the simulations which assume the simple one-step QFS reaction mechanism. The experimental responses and acceptances for all final-state particles are taken into account in the simulation. The integral of the experimental distribution in each panel represents the fraction of the total accepted cross section and is indicated by the weight factor V, defined as $V = N_{Qt}/N_{acc} * 100\%$ where N_{Qt} is the number of events observed within the selected t-Q_{rf} range, and N_{acc} is the total number of accepted $^{12}C(p,2p)^{11}B$ events. By construction, the sum of all V values is proportional to the total accepted cross section of 11.8(13) mb. This value is obtained from the total reaction cross section 19.2(18)(12) mb reported in Panin et al. [21], scaled by the experimental acceptance of 61.7%, as estimated from the present simulations. The simulated distributions are normalized to the experimental data, and the reduced chi-squared value χ^2_ν is indicated in each panel, while the error bars represent the statistical uncertainties.

5. Discussion

As commonly acknowledged in the literature (see *e.g.* [29,32,33,37]), fulfillment of the Treiman-Yang test provides a necessary though not sufficient condition for the validity of the impulse approximation. For example, Kolybasov et al. [29] pointed out that, under certain conditions and approximations, some triangular graphs, such as those shown in Fig. 1b, may also satisfy this condition. Nevertheless, the systematic analysis of the reaction kinematics presented in this work, together with the overall good agreement between the experimental Φ_{TY} distributions and the simulations shown in Figs. 5a and 7 provide strong evidence for the dominance of the pole mechanism.

At the same time, a careful inspection of the distributions and the corresponding χ^2_ν values in Fig. 7 indicates noticeable deviations in the regions characterized by small and large t values with Q_{rf} larger than 200 MeV/c, where the discrepancies between experimental and simulated distributions appear to exceed the level expected from purely statistical fluctuations. The integrated yield of the panels with $\chi^2_\nu > 3$ corresponds to approximately 17.3% of the total accepted cross section, whereas the remaining part of the data is generally well reproduced by the simulations. Several sources of systematic uncertainty may contribute to these deviations. In particular, reactions induced by the carbon content of the CH_2 target cannot be fully excluded. Owing to the limited statistics collected with the dedicated carbon target, a differential subtraction of the carbon-induced background for each individual t-Q_{rf} panel is presently not feasible. Nevertheless, as discussed in Section 3, the overall contribution of the carbon-induced reactions within the applied experimental cuts is on the order of 9%, which can be accounted for as a systematic uncertainty. Additional studies based on variations of the experimental cuts and alternative analysis procedures indicate that the resulting systematic distortions of the Treiman–Yang distributions do not exceed approximately 10%.

It should also be emphasized that the experimental data are compared with Monte-Carlo simulations based on a simplified QFS reaction model. In particular, the virtual p-p scattering cross section is assumed to be isotropic and constant in the p-p center-of-mass frame for all kinematic configurations. This approximation is motivated by the experimentally known behavior of free p-p scattering cross sections, which remain nearly isotropic and weakly dependent on energy in the range relevant to the present study. Despite the overall close agreement between the model and the experimental data, more sophisticated theoretical calculations may still be required, especially for a more accurate description of the θ^*_{pp} distribution in Fig. 4.

6. Summary and conclusions

Large-acceptance experiments in inverse kinematics offer a convenient experimental configuration to study the detailed features of the QFS reaction mechanism. In the present work, the reaction $^{12}C(p,2p)^{11}B$ at 400 MeV/nucleon was studied as a benchmark case, and a systematic Treiman-Yang test was performed for the first time. By reconstructing the complete reaction kinematics from an incomplete set of observables, the reaction mechanism could be investigated in considerable detail. In particular, the angular information of the recoil protons was combined with the momentum vector of the heavy (A-1) residue to determine the essential kinematic quantities characterizing the underlying p-p scattering process. This made it possible to extract distributions of the Treiman-Yang angle for different regions of missing and transfer momenta and thereby test the validity of the impulse approximation. The obtained results provide strong evidence that the dominant fraction of the observed reactions proceeds through the pole mechanism characteristic of quasi-free scattering.

Data availability

Data will be made available on request.

Declaration of competing interest

The authors declare that they have no known competing financial interests or personal relationships that could have appeared to influence the work reported in this paper.

Acknowledgements

The authors acknowledge support from HMWK through the LOEWE center HIC for FAIR, the GSI-TU Darmstadt cooperation agreement, the BMBF under Contracts No. 05P12RDFN8 and 05P21RDFN1, the Helmholtz Alliance EMMI, the Swedish Research Council, the U.S. NS Grant No. 1415656, the Spanish research agency CICYT under Project No. FPA2009-07387, the Royal Society and the UK STFC under grant numbers ST/L005727/1, ST/P003885/1 and ST/V001035/1. (C.A.B.) acknowledges support by the DOE grant No. DE-SC0026074 and by the ExtreMe Matter Institute EMMI at the GSI Helmholtzzentrum für Schwerionenforschung. V.P. acknowledges enlightening discussions with Dr. Tomohiro Uesaka.

References

[1] T. Aumann, et al., Quenching of single-particle strength from direct reactions with stable and rare-isotope beams, Prog. Part. Nucl. Phys. 118 (2021) 103847. https://doi.org/10.1016/j.ppnp.2021.103847
[2] V. Panin, T. Aumann, C.A. Bertulani, Quasi-free scattering in inverse kinematics as a tool to unveil the structure of nuclei, Eur. Phys. J. A 57 (3) (2021) 103. https://doi.org/10.1140/epja/s10050-021-00416-9
[3] L. Atar, R3B Collaboration, Quasifree (p,2p) reactions on oxygen isotopes: observation of isospin independence of the reduced single-particle strength, Phys. Rev. Lett. 120 (5) (2018) 052501. https://doi.org/10.1103/PhysRevLett.120.052501
[4] M. Holl, R3B Collaboration, Quasi-free neutron and proton knockout reactions from light nuclei in a wide neutron-to-proton asymmetry range, Phys. Lett. B 795 (2019) 682–688. https://doi.org/10.1016/j.physletb.2019.06.069
[5] S. Chen, et al., Level structures of ^{56,58}Ca cast doubt on a doubly magic ^{60}Ca, Phys. Lett. B 843 (2023) 138025. https://doi.org/10.1016/j.physletb.2023.138025
[6] I. Syndikus, R3B Collaboration, Probing the Z = 6 spin-orbit shell gap with (p,2p) quasi-free scattering reactions, Phys. Lett. B 809 (2020) 135748. https://doi.org/10.1016/j.physletb.2020.135748
[7] A. Corsi, et al., Searching for universality of dineutron correlation at the surface of Borromean nuclei, Phys. Lett. B 840 (2023) 137875. https://doi.org/10.1016/j.physletb.2023.137875
[8] S. Paschalis, et al., Nucleon-nucleon correlations and the single-particle strength in atomic nuclei, Phys. Lett. B 800 (2020) 135110. https://doi.org/10.1016/j.physletb.2019.135110
[9] M. Patsyuk, et al., Unperturbed inverse kinematics nucleon knockout measurements with a carbon beam, Nat. Phys. 17 (6) (2021) 693–699. https://doi.org/10.1038/s41567-021-01193-4
[10] P.J. Li, et al., Validation of the ^{10}Be ground-state molecular structure using ^{10}Be (p,pα)^{6}He triple differential reaction cross-section measurements, Phys. Rev. Lett. 131 (21) (2023) 212501. https://doi.org/10.1103/PhysRevLett.131.212501
[11] M. Duer, et al., Observation of a correlated free four-neutron system, Nature 606 (7915) (2022) 678–682. https://doi.org/10.1038/s41586-022-04827-6
[12] Y. Kondo, et al., First observation of ^{28}O, Nature 620 (7976) (2023) 965–970. https://doi.org/10.1038/s41586-023-06352-6

[13] P. Kitching, et al., Recent developments in quasi-free nucleon-nucleon scattering, Adv. Nucl. Phys. 15 (1985) 43.
[14] T. Wakasa, K. Ogata, T. Noro, Proton-induced knockout reactions with polarized and unpolarized beams, Prog. Part. Nucl. Phys. 96 (2017) 32–87. https://doi.org/10.1016/j.ppnp.2017.06.002
[15] G. Jacob, T.A. Maris, Quasi-free scattering and nuclear structure, Rev. Mod. Phys. 38 (1) (1966) 121–142. https://doi.org/10.1103/RevModPhys.38.121
[16] G. Jacob, T.A. Maris, Quasi-Free scattering and nuclear structure. II, Rev. Mod. Phys. 45 (1) (1973) 6–21. https://doi.org/10.1103/RevModPhys.45.6
[17] T. Aumann, C.A. Bertulani, J. Ryckebusch, Quasifree (p,2p) and (p,pn) reactions with unstable nuclei, Phys. Rev. C 88 (6) (2013) 064610. https://doi.org/10.1103/PhysRevC.88.064610
[18] E. Byckling, K. Kajantie, Particle kinematics, University of Jyvaskyla, Jyvaskyla, Finland, 1971.
[19] T. Uesaka, On the kinematics of (p, pX) knockout reactions in normal and inverse kinematics, Prog. Theor. Exp. Phys. 2024 (8) (2024) 083D01. https://doi.org/10.1093/ptep/ptae013
[20] T. Kobayashi, K. Ozeki, K. Watanabe, Y. Matsuda, Y. Seki, T. Shinohara, T. Miki, Y. Naoi, H. Otsu, S. Ishimoto, S. Suzuki, Y. Takahashi, E. Takada, (p,2p) reactions on $^{9-16}$C at 250 MeV/A, Nucl. Phys. A 805 (1-4) (2008) 431–438. https://doi.org/10.1016/j.nuclphysa.2008.02.282
[21] V. Panin, et al., Exclusive measurements of quasi-free proton scattering reactions in inverse and complete kinematics, Phys. Lett. B 753 (2016) 204–210. https://doi.org/10.1016/j.physletb.2015.11.082
[22] H.N. Liu, et al., STRASSE: a silicon tracker for quasi-free scattering measurements at the RIBF, Eur. Phys. J. A 59 (6) (2023) 121. https://doi.org/10.1140/epja/s10050-023-01018-3
[23] A.W. Stetz, Analysis of quasi-free scattering data in the impulse approximation, Phys. Rev. C 21 (5) (1980) 1979–1988. https://doi.org/10.1103/PhysRevC.21.1979
[24] M. Holl, et al., Border of the island of inversion: unbound states in ^{29}Ne, Phys. Rev. C 105 (3) (2022) 034301. https://doi.org/10.1103/PhysRevC.105.034301
[25] A. Frotscher, et al., Sequential nature of (p,3p) two-proton knockout from neutron-rich nuclei, Phys. Rev. Lett. 125 (1) (2020) 012501. https://doi.org/10.1103/PhysRevLett.125.012501
[26] S.B. Treiman, C.N. Yang, Tests of the single-pion exchange model, Phys. Rev. Lett. 8 (3) (1962) 140–141. https://doi.org/10.1103/PhysRevLett.8.140
[27] L.V. Chulkov, et al., Quasi-free scattering with ^{6,8}He beams, Nucl. Phys. A 759 (1) (2005) 43–63. https://doi.org/10.1016/j.nuclphysa.2005.05.148
[28] B. Debebe, et al., Reaction ^{2}H(p,dπ^{+})n at 506 MeV, Phys. Rev. C 31 (5) (1985) 1841–1852. https://doi.org/10.1103/PhysRevC.31.1841
[29] V.M. Kolybasov, G.A. Leksin, I.S. Shapiro, REVIEWS OF TOPICAL PROBLEMS: The direct reaction mechanism at high energies, Sov. Phys. Uspekhi 17 (3) (1974) 381–404. https://doi.org/10.1070/PU1974v017n03ABEH004140
[30] A.M. Baldin, V.I. Goldanskii, I.L. Rozenthal, Kinematics of nuclear reactions, Oxford University Press, Amen House, London E.C.4, 1961.
[31] G. Källén, Elementary Particle Physics, Reading, MA, Addison-Wesley, 1964.
[32] I.S. Shapiro, V.M. Kolybasov, G.R. Augst, Treiman-Yang criterion for direct nuclear reactions, Nucl. Phys. 61 (3) (1965) 353–367. https://doi.org/10.1016/0029-5582(65)90097-0
[33] R. Corfu, et al., Treiman-Yang criterion for quasifree scattering in deuteron breakup at low energy, Phys. Rev. Lett. 27 (24) (1971) 1661–1664. https://doi.org/10.1103/PhysRevLett.27.1661
[34] P.G. Fallica, et al., Treiman-Yang criterion as a test of the pole approximation in the ^{9}Be(^{3}He,$\alpha\alpha$)^{4}He reaction, Phys. Rev. C 24 (4) (1981) 1394–1399. https://doi.org/10.1103/PhysRevC.24.1394
[35] W. Von Witsch, et al., Test of the Treiman-Yang criterion in the ^{2}H(d, pd)n reaction at 20 MeV bombarding energy, Nucl. Phys. A 195 (2) (1972) 617–622. https://doi.org/10.1016/0375-9474(72)91083-4
[36] C. Spitaleri, et al., The ^{3}He + ^{5}He$\rightarrow\alpha+\alpha$ reaction below the Coulomb barrier via the Trojan Horse Method, Eur. Phys. J. A 57 (1) (2021) 20. https://doi.org/10.1140/epja/s10050-020-00324-4
[37] S.I. Sidorchuk, et al., Study of the ^{6}He structure in the reaction of quasifree scattering ^{4}He(^{6}He, 2 α), Nucl. Phys. A 840 (1) (2010) 1–18. https://doi.org/10.1016/j.nuclphysa.2010.04.002